INFLUENCE OF ROUNDED LEADING EDGE ON THE FLOW SEPARATION BY DNS

Jorge Silvestrini, jorgehs@pucrs.br
Faculdade de Engenharia, Pontifícia Universidade Católica do Rio Grande do Sul
Av. Ipiranga, 6681, Porto Alegre, RS
90619-900, Brasil

Eric Lamballais, eric.lamballais@univ-poitiers.fr
Laboratoire d'Etudes Aérodynamiques UMR 6609, Université de Poitiers, CNRS
Téléport 2 - Bd. Marie et Pierre Curie B.P. 30179
86962 Futuroscope Chasseneuil Cedex, France

Sylvain Laizet, s.laizet@imperial.ac.uk
Institute for Mathematical Sciences and Department of Aeronautics, Imperial College London
53 Princes Gate, Exhibition Road, South Kensington Campus
London SW7 2PG, UK

Abstract. *The flow separation of a uniform flow induced by a two-dimensional obstacle with rounded leading-edge is studied by direct numerical simulation (DNS). The main purpose is to analyse the flow dynamics of the recirculation bubble for different curvatures levels. Four cases are investigated corresponding to more or less rounded leading-edge. The Reynolds number, based on the free-stream velocity and the height of the obstacle, is equal to* 2000 *for all the simulations. This value demands a great effort on grid resolution and massively parallel supercomputers are used to guarantee the feasibility of a DNS. Results show that curvature deeply influence the separation bubble dynamics with a significant increase of the separation angle and hence, the height of the bubble, as the curvature ratio decreases. Secondary bubble recirculation is observed as the obstacle leading edge is less rounded. Turbulent statistics of Reynolds stresses, kinetic energy and production term are also influenced by curvature effects. Although the leading-edge flow separation, identified by instantaneous visualizations, seems to be a two-dimensional mechanism, the spanwise Reynolds stress tends to dominate the other components in the upstream region of the bubble as the curvature increases. The maxima value of kinetic energy moves downstream toward the reattachment point as the curvature level decreases while high curvature cases produce higher levels of velocity fluctuations. This is also observed in the power spectra of streamwise velocity fluctuations from time series recorded further downstream the reattachment zone.*

Keywords: *separation bubble, vortex dynamics, direct numerical simulations.*

1. INTRODUCTION

The flow separation produced by a leading edge curvature is a typical flow configuration that occurs in many practical applications like road vehicles and aircraft aerodynamics and civil engineering. While flow separation in aerodynamics is mainly important to account for drag and noise production, in civil engineering of buildings, it is responsible for pressure fluctuations resulting in vibrations that may damage the structure.

Although the subject is of great interest, results on flow separation considering curvature effects seem to be very scarse. In this paper the influence of the leading edge curvature on a uniform flow is studied by means of direct numerical simulations (DNS). Flow separation from 2D and 3D obstacles were considered previously by Lamballais *et al.* (2008). For these numerical simulations, the combined effect of aspect ratio and curvature was taken into account for a Reynolds number, based on the free-stream velocity and the height of the obstacle, equal to 1250. Results show good qualitative and quantitative agreement with previous experiments (Courtine *et al.*, 2007), in particular, the recirculation bubble formation shows similar topological features. Special attention was given to the sensitivity to upstream conditions considering different levels of inflow fluctuations. It was found that strong curvature reduces drastically the upstream receptivity of the flow, phenomena which were interpreted in terms of convective/absolute instability.

Additionally to these numerical simulations, new DNS for purely 2D bodies with a larger range of curvature cases were performed for a Reynolds number of 2000 while the DNS strategy was maintained (Lamballais *et al.* 2009). This improvement of our results in terms of realism has required to increase drastically the computational effort with the help of the new generation of supercomputers using massively parallel architectures. The aim of this work wasto investigate the influence of the shape of the body on the bubble formation and on the receptivity of the flow to inflow conditions. For this purpose, 16 calculations depending on the leading-edge curvature, the 2D/3D nature of the flow and on the inflow perturbations were finally retained. First results show a separating-reattaching flow with a common feature of self-excitation in the separation bubble revealed by the ability of every flow to lead to self-sustaining unsteady processes

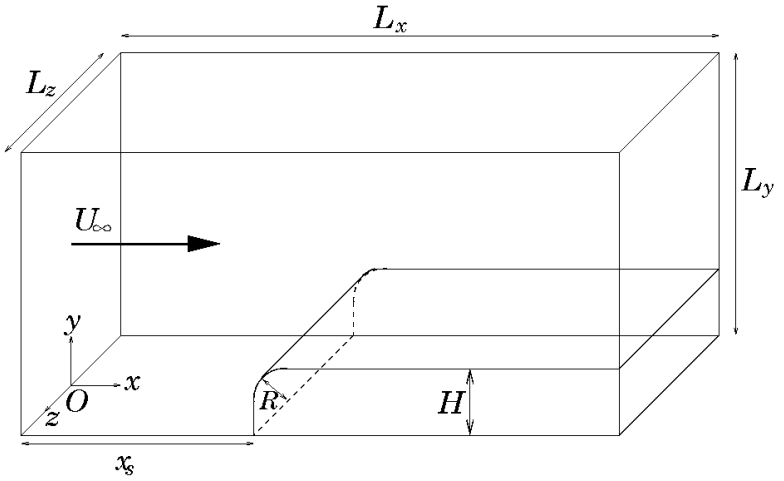

Figure 1. Schematic view of the flow configuration.

without the need of any inlet excitation. Despite this common property, the single change of the front-edge curvature is found to deeply influence the bubble dynamics (Lamballais *et al.* 2009).

In this paper, new results for these numerical simulations are presented, focusing on additional characteristics of the recirculation bubble, the computation and analysis of turbulent statistics and frequency analysis from time series related to different curvatures levels. Only cases with non-zero inflow perturbations are considered.

2. FLOW CONFIGURATION AND NUMERICAL METHODS

Figure 1 shows the flow configuration considered. The two-dimensional obstacle is completely defined through the (x, y) location on the stagnation point $(x_s, 0)$, its height H and its constant edge radius R. A single non-dimensional parameter $\eta = R/H$ is defined while cases corresponding to $\eta = 0.125, 0.25, 0.5, 1$ are selected. For present DNS calculations, the following boundary conditions are used: inflow/outflow conditions are imposed in the streamwise direction (velocity boundary conditions of Dirichlet type at the inlet), in the vertical direction free-slip conditions are used while periodicity is retained for the spanwise direction.

The incompressible Navier-Stokes equations are solved using a recent version of `Incompact3d`, adapted to massively parallel supercomputers (Laizet *et al.*, 2008). This code is based on compact sixth-order finite difference schemes for the spatial differentiation, a second order Adams-Bashforth for the time integration while the incompressibility condition is imposed through the full resolution of a Poisson equation for the pressure in spectral space. For validation purposes, this new version of the numerical code was successfully tested in different academic configurations (see Laizet and Lamballais, 2009)

The computational domain $L_x \times L_y \times L_z = 20.25H \times 16H \times 6H$ is discretized on a Cartesian grid (stretched in y). The presence of the body is modelled with an immersed boundary method adapted to the use of high-order schemes (Parnaudeau *et al.* 2008). Two types of computational grid are used depending on the curvature. For cases corresponding to $\eta = 0.25, 0.50, 1$, the resolution used was $n_x \times n_y \times n_z = 1621 \times 451 \times 300$ mesh nodes while for the high curvature case, $\eta = 0.125$, a grid resolution $n_x \times n_y \times n_z = 3241 \times 901 \times 300$ mesh nodes was required. This spatial resolution ensures to describe the rounded edge geometry using at least 20 mesh nodes by curvature radius.

The inflow velocity U_∞ is perturbed by a low amplitude noise $u' \approx 0.1\%U_\infty$ computed to excite randomly and equally (in average) all the length scales up to a cutoff wavelength of $H/6$. The time periodicity of this generated noise is $T = 40H/U_\infty$. Statistics are collected on a duration multiple of this particular time period (after a transient stage to obtain a well established flow) with an additional average in the homogeneous z-direction. The marginal statistical convergence reached by 3D DNS using only a single period $T = 40H/U_\infty$ has been considered enough as far as the following analyses are concerned. Naturally, a quantitative study of low frequency phenomena would require to consider a clearly larger integration time to provide accurate statistics.

3. RESULTS

As already mentioned, results of four DNS each one corresponding to a curvature level $\eta = 0.125, 0.25, 0.5, 1$ will be analysed here.

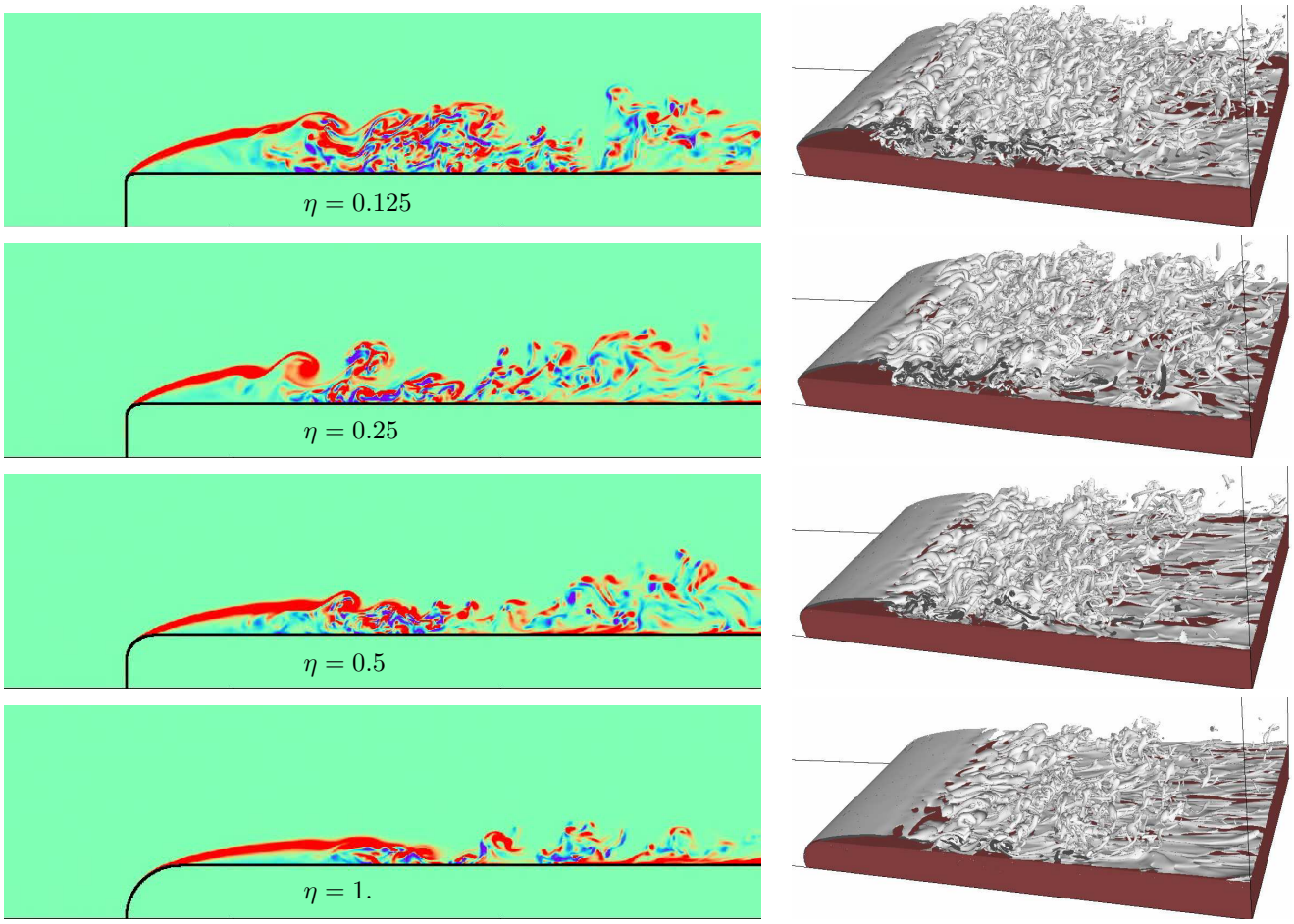

Figure 2. Maps of spanwise vortcity ω_z and perspective views of vorticity modulus isosurface $\omega = 8U_\infty^2/H$ for $\eta = 0.125, 0.25, 0.50, 1$ (from top to bottom).

3.1 Instantaneous flow visualization

Firstly, some pictures taken at the end of the numerical simulations for the four curvatures are presented in Fig. 2. The left-side pictures show maps of instantaneous spanwise vorticity at the middle spanwise plan ($z = 0$). The global characteristics of the flow separation start by a laminar boundary layer that detaches leading to a shear layer. In presence of small perturbations, the shear layer is submitted to Kelvin-Helmholtz (KH) instability with formation of vortices. These KH vortices, that may eventually pair, enclosed a highly intermittent recirculation zone to finally reattach on the obstacle surface in some $x-$position developing a turbulent boundary layer further downstream. The influence of different curvature ratio is clearly seen in Fig. 2. The prominent feature seems to be the increase of the separation angle as the obstacle becomes less rounded. This behaviour increases the height of the recirculation bubble leading to higher levels of spanwise vorticity above the obstacle surface. From movies taken during all the simulations, it seems that the reattachment zone is highly intermittent that leads to a difficult estimation of the recirculation length from instantaneous fields. Another striking feature that is observed from movies is the perceptible increase of streamwise recirculation velocity (the backflow) inside the bubble as the curvature increases.

On the right-side of Fig. 2, pictures for an iso-surface of vorticity modulus are observed for the four curvatures selected. This kind of images allows us to investigate more in details the 2D phenomena previously observed, showing the full 3D flow dynamics (for an iso-value chosen). A first observation from these pictures is the fairly 3D nature of the KH vortices shedded while the separation region seems to be controlled by two-dimensional mechanism due to the 2D obstacle considered. The figure denotes that the "first" KH vortices detached in the free-shear layer are less two-dimensional when η decreases. Downstream, the mixing layer is highly deformed leading to streamwise vorticity formation with a notably increase of three-dimensional motions through breakdown processes. Comparisons between the different body geometries show that the separation is deeply modified by the shape of the front edge with a more marked turbulent region when the curvature is high. The resulting levels of vorticity seem to be increased accordingly with a simultaneous scale reduction of the vortical structures, leading to the feeling that the Reynolds number is higher as η

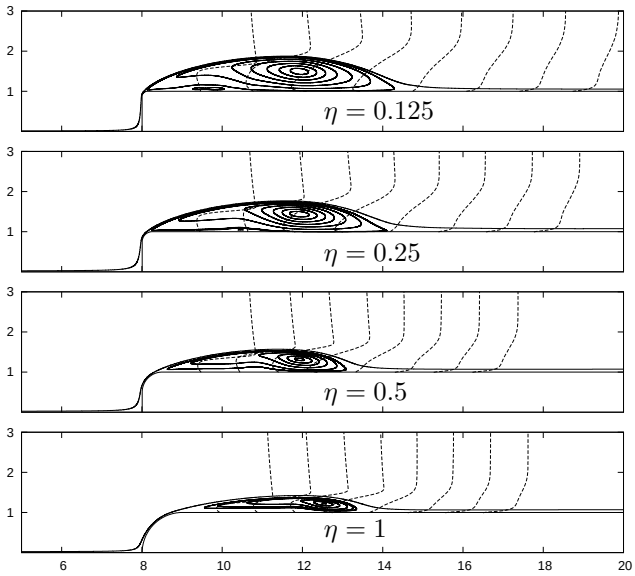

Figure 3. Mean streamlines with profiles of mean streamwise velocities at x/l_r for 0.2 to 1.6 each 0.2 for $\eta = 0.125, 0.25, 0.50, 1$ (from left to right and top to bottom respectively).

decreases. Present visualizations suggest that the reduction of η increases the turbulence activity inside the separation bubble through physical mechanisms involving the direct excitation of the separated shear-layer.

3.2 Mean flow description

The two-dimensional mean (in time and in the homogeneous $z-$direction) velocity field may be used to describe the geometrical characteristics of the recirculation region. Three parameters are concerned here: the bubble length l_r, the bubble height h_r and the separation angle θ. These parameters can be computed in different ways. Here l_r is estimated as $x_r - x_0$ where x_r is the streamwise location where the mean flow reattaches (detected here via the sign change of the longitudinal mean velocity at the first mesh node above the wall) while x_0 corresponds to the end location of the body curvature ($x_0 = x_s + R$) where the separation is nearly observed for all the cases considered here (see Fig.1). The bubble height h_r and the separation angle θ are computed from the mean streamlines through the use of the delimiting streamline of the recirculation bubble. This streamline is defined as the first streamline shot from the inlet that does not enter in the bubble. Fig. 3 shows some mean streamlines denoting the recirculation bubble along with profiles of mean streamwise velocity for selected $x-$stations . Table 1 summarizes the values obtained for each curvature considered.

η	0.125	0.25	0.50	1
l_r	6.63	5.94	4.83	4.68
h_r	.88	.77	.57	.42
θ	40°	32°	23°	15°
$U_{\min}$	-.38	-.35	-.30	-.24
$k_{\max}$	.16	.16	.14	.10

Table 1. Recirculation length l_r, separation bubble height h_r, separation angle θ, minimum value of the mean longitudinal velocity $U_{\min}$ (highest backflow intensity), maximum of the turbulent kinetic energy $k_{\max}$. Present results are normalized by H and U_∞.

In terms of curvature effects, the reduction of η is found to increase significantly l_r (up to +40%). The bubble height h_r seems to be the more sensible value to the variation of η as it duplicates between extremes curvatures (from $0.42H$ to $0.88H$) as η decreases. Similar trends follow the separation angle θ which varies from 15° at low curvature ($\eta = 1$) to 40° at the highest curvature concerned here ($\eta = 0.125$). This change of the separation orientation leads logically to an increase of h_r when the curvature is increased. Table 1 also shows the increase of the maxima values for the mean streamwise recirculation velocity, that is the backflow, as the curvature increases (η decreases).

Fig. 3 shows also profiles of streamwise velocities at selected stations normalized by the recirculation bubble length. These profiles denote the spreading rate of the free shear layer for different curvatures.

For comparison purposes, the l_r obtained for $\eta = 1$ is in good agreement with the value, $lr = 5.2H$, computed in the large-eddy simulation (LES) of Yang and Voke (2001) for $Re = 1725$. A more significant underestimation is

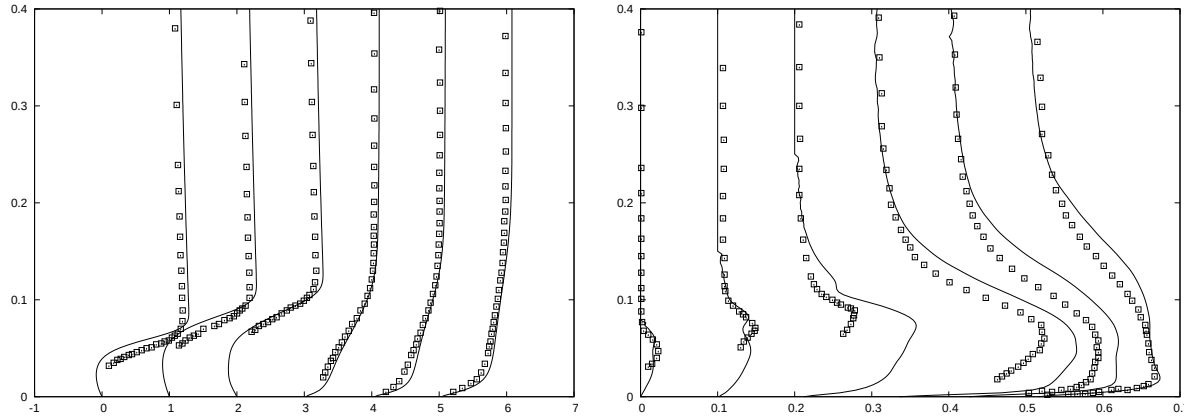

Figure 4. Mean streamwise velocity (left) and streamwise velocity fluctuations (right) at x/l_r =0.22, 0.44, 0.66, 1.09, 1.27 and 1.64 for $\eta = 1$. Solid lines are present DNS while square symbols correspond to experimental data (Yang and Voke, 2001).

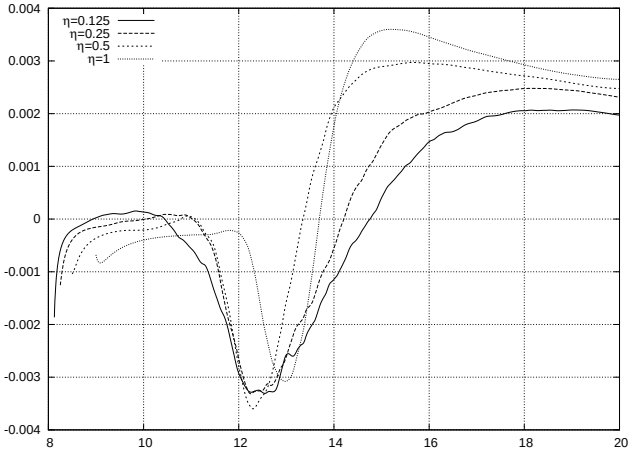

Figure 5. Friction coefficient C_f for $\eta = 0.125, 0.25, 0.50, 1$.

found in this work for l_r at $\eta = 0.125$ by comparison with the typical value $l_r = 10H$ reported in the literature at higher Reynolds number for a sharp edge (Kiya and Sasaki, 1985; Suksangpanomrung *et al.*, 2000; Abdalla and Yang, 2004). Considerations about the level of inflow perturbations, curvature and perhaps, on Reynolds number, may partially explain this difference. Another source that may influence for this particular case ($\eta = 0.125$) is the marginal statistical convergence reached for this very high time consuming computation.

In Yang and Voke (2001), the authors compared their LES results of mean axial velocity and root mean square (rms) of streamwise velocity fluctuation at selected streamwise stations with unpublished experimental data of J.Coupland (measured using hot-wire probe). In Fig. 4 this comparison is reproduced with the DNS results computed here (instead of the LES results) with a renormalization by the bubble recirculation length. Fairly good agreement is obtained between the experimental and the DNS data. Differences in blockage ratio could explain the difference observed in the free-stream velocity. For the rms fluctuations, the main differences are observed near the reattachment point where the DNS results show higher values of streamwise fluctuations. Uncertainties due to levels of inflow velocity fluctuations and Reynolds number may explain these differences. Further downstream, the agreement seems to be much better.

Regarding furthermore to Fig. 3, a more complex structure of the separation bubble is observed particularly for $\eta = 0.125, 0.25$. The figure shows some streamlines denoting counterclockwise secondary recirculation. To better identify the occurrence of secondary structures for all the cases considered, the streamwise variation of the mean friction coefficient for the four curvatures is plotted in Fig.5. For simplicity reason, only the horizontal part of the obstacle is retained. The picture denotes a sign change of the mean wall shear stress for $\eta = 0.125, 0.25$ and $\eta = 0.50$ for $9 \leq x \leq 11$. This fact confirms that secondary motion should exist for the concerned curvatures. Moreover these secondary structures move upstream and increase their intensity as η decreases. Clearly, no secondary motion should be expected for $\eta = 1$ since no sign change of friction coefficient is observed for this curvature near the upstream region of the bubble. Fig. 5 also allows another way of l_r computation, which gives exactly the same values as it was computed in

Table 1.

3.3 Turbulent statistics

Fig. 6 summarizes the results obtained for the normal Reynolds stresses components $\overline{u'u'}, \overline{v'v'}, \overline{w'w'}$ and for the shear one $-\overline{u'v'}$. The selected contours lines, for the four components, are 0.001, 0.01, 0.02, then by step of 0.02. In these figures it was superposed a dash line denoting the delimiting recirculation bubble streamline.

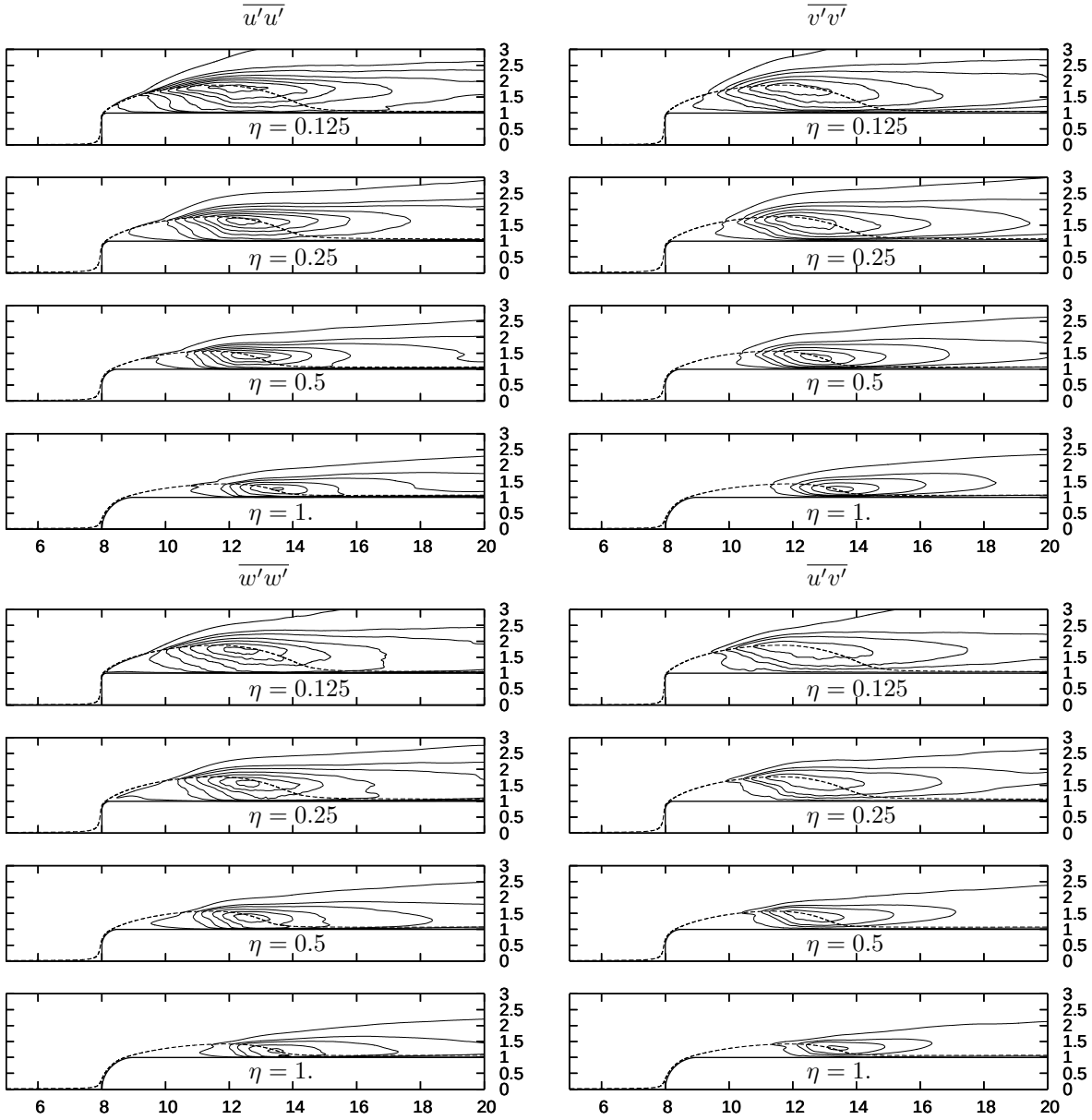

Figure 6. Normal $\overline{u'u'}$, $\overline{v'v'}$, $\overline{w'w'}$, and shear $-\overline{u'v'}$ Reynolds stress contours for $\eta = 0.125, 0.25, 0.5, 1$ (from top to bottom). The dash line denotes the delimiting bubble recirculation streamline. Contours levels for 0.001, 0.01, 0.02 then by step of 0.02.

Some general trends could be observed in the figure. Firstly, for all the components computed, their maxima values which are located at the boundary of the bubble, move downstream to the reattachment zone as the obstacle become more rounded (η increases). These locations may be related to the recirculation bubble centre with follow similar trends toward the reattachment zone for low curvature (see Fig. 3).

Fig. 6 also denotes that the turbulence levels rise as the curvature is increased, characteristic observed in previous qualitative analysis from instantaneous visualization (Fig. 2). In particular, the more significant non-zero isoline, here taken from the threshold value of 0.1%, moves toward the separation point as η decreases.

In addition to the shift of its maximum toward the reattachment, the $\overline{w'w'}$ Reynolds stress component shows a specific feature in terms of curvature sensitivity in the separation region. Fig. 6 reveals that when the curvature is increased,

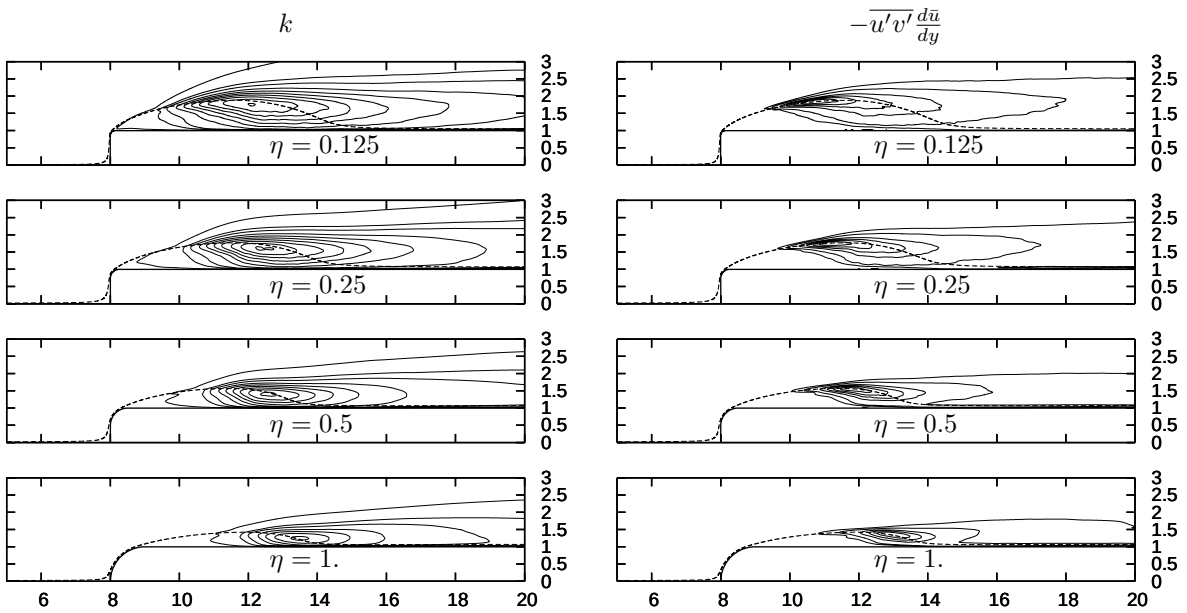

Figure 7. Turbulent kinetic energy k and production term $-\overline{u'v'}\frac{d\bar{u}}{dy}$ contours for $\eta = 0.125, 0.25, 0.5, 1$. The dash line denotes the delimiting bubble recirculation streamline.

very high levels of spanwise velocity fluctuations are present in the neighbourhood of the separation line. This effect is so marked that for $\eta = 0.125$, w-fluctuations are found to dominate the two other components in the near-separation region. This drastic change of Reynolds stress tensor anisotropy cannot be interpreted as a consequence of the primary instabilities that develop further downstream in the shear layer region. The source of w-fluctuations could be instead attributed to the transport of turbulent 3D fluctuations from the reattaching region by the reverse flow that is stronger for high curvature. This interpretation should be quantitatively confirmed through a complete analysis of the Reynolds stress budget. However, the identification of strong w-fluctuations from the start of the separation at high curvature provides, at least partially, an explanation of the more 3D nature of the primary Kelvin-Helmoltz structures in this case as observed in Fig. 2 (see especially the case $\eta = 0.125$). The 3D excitation of the detached shear layer, clearly more effective for high value of η, contributes to trigger 3D instabilities while favouring a rapid turbulent breakdown.

As a summary of the results shown in Fig. 6 for the normal Reynolds stress components, the left side of Fig. 7, presents the contour lines corresponding to the kinetic energy k for the four curvatures. All the results related for the normal Reynolds stress components are, of course, reproduced here. In particular, the values corresponding to the maxima kinetic energy computed for each case (see Table 1), quantify the increase of turbulence activity as the curvature increases.

As the main expected source of turbulent kinetic energy, a map of the production term $-\overline{u'v'}\frac{d\bar{u}}{dy}$ is presented in Fig. 7. For all the curvatures, maxima values for the production term computed, is highly concentrated on the boundary of the recirculation bubble. The striking difference between the low and high curvature cases concerns the location of the production maximum that is found near the reattachment for $\eta = 1$ whereas for $\eta = 0.125$, the production is found to occur mainly in the detached shear layer. This drastic change of production region confirms that the dynamics of the separation bubble is governed by different mechanism depending on the curvature.

3.4 Frequency analysis

Time series for the three velocity components were recorded in different stations above the obstacle. Results for the power spectra of streamwise velocity fluctuations at the location $(x, y) = (17H, 1.75H)$, that is further downstream to the reattachment zone, are plotted in Fig. 8 for the four curvatures. Frequencies are normalized by the free-stream velocity and the obstacle height. First observations from the picture reproduce the previous observations about the increase of kinetic energy contents as the curvature increases (η decreases). The spectral analysis of streamwise velocity fluctuations shows that the turbulence is significantly more developed inside as well as behind the separation bubble for high curvature. Frequency analysis denotes high levels of streamwise velocity fluctuations for low frequencies when η decreases.

In the LES computations of Yang and Voke (2001) for $\eta = 1$, the authors reported shedding processes occurring within a range of frequencies and estimated the average value at about $0.18U_\infty/H$. Peak values of Strouhal number nearly $f = 0.2U_\infty/H$ may be identified in Fig. 8 not only for $\eta = 1$ but also for the others cases. Others peaks corresponding to harmonic components, for instance, $f = 0.4U_\infty/H$, may be also observed in the figure.

Even if each spectrum corresponds to low-Reynolds turbulence, it can be observed a narrow inertial zone at $\eta = 0.125$ while for $\eta = 1$, in a the same spectral range, the spectrum is found to be steeper.

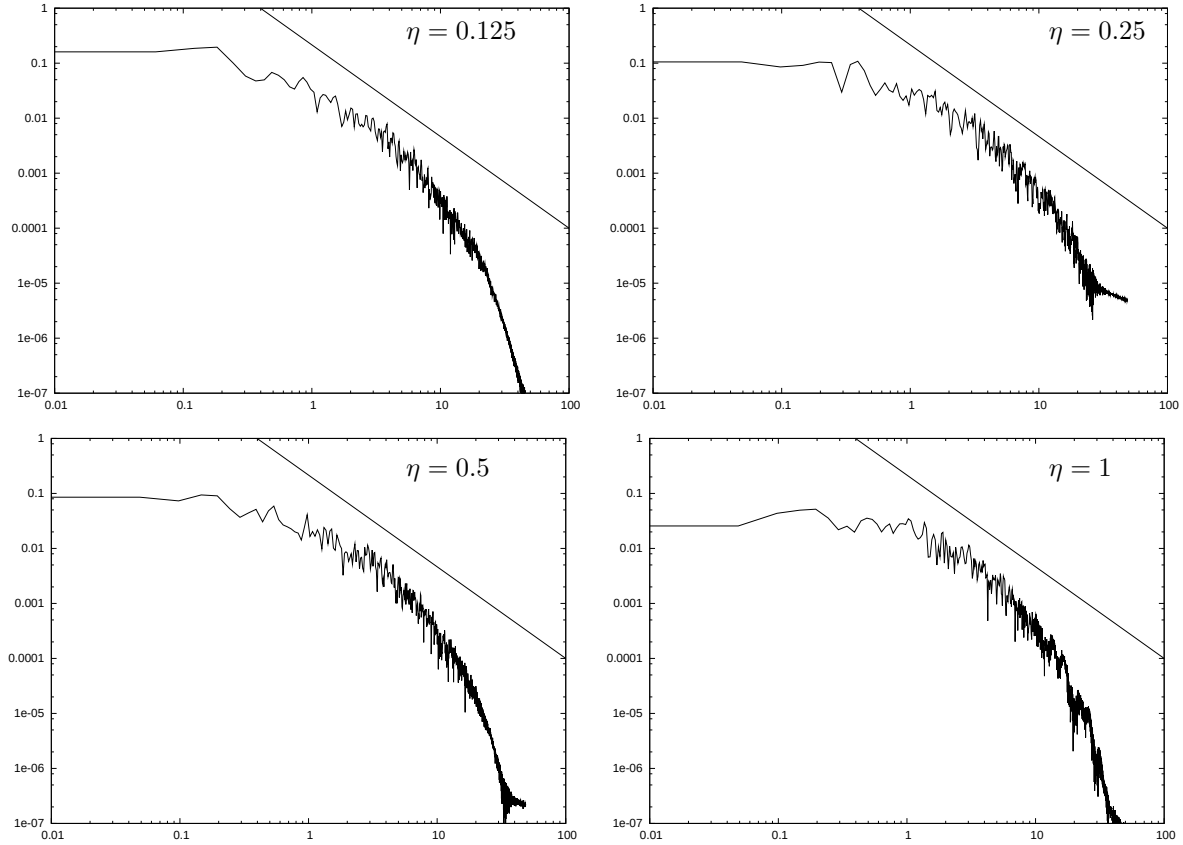

Figure 8. Power spectra of streamwise velocity fluctuations u' at $(x, y) = (17, 1.75)$ for $\eta = 0.125, 0.25, 0.5, 1$. The straight line denotes a $-5/3$ slope.

4. CONCLUSION

The flow separation induced by a two-dimensional obstacle with different rounded leading-edge was studied by direct numerical simulation for a Reynolds number, based on the free-stream velocity and the obstacle height, of $Re = 2000$. Four curvatures cases were considered corresponding to $\eta = R/H = 0.125, 0.25, 0.5, 1$. The Reynolds number combined with the resolution needed for the front edge required to simulate the flow, demanded a great effort on grid resolution and the use of massively parallel supercomputers to guarantee the feasibility of a DNS. The high curvature case requires to simulate the flow up to 876 million of mesh nodes.

For all the cases treated here, a separating-reattaching flow is obtained with a common feature of self-excitation in the separation bubble. Despite this common property, the single change of the front-edge curvature is found to deeply influence the bubble dynamics. As the curvature ratio decreases, results from the mean flow show a a significant increases of the separation angle and the height of the bubble. These features may be also observed from instanteanous visualizations and movies taken during the simulation. The recirculation bubble length also increases with the curvature. As the curvature increases (η decreases), the Kelvin-Helmholtz vortices formed in the separated shear layer seem to be less two-dimensional. This feature denotes a 3D mechanism which may be related to the growing of spanwise fluctuations in the upstream region of the bubble transported from the reattachment region by the intense streamwise recirculation backflow (38% of U_∞ for $\eta = 0.125$).

Counterclockwise bubble recirculation is observed as the obstacle leading edge is less rounded. Even for intermediate curvature ($\eta = 0.50$) the streamwise variation of the friction coefficient confirms the presence of such a recirculation in the upstream region of the bubble. No secondary motion is observed for $\eta = 1$.

Turbulent statistics of Reynolds stresses, kinetic energy and production term are also influenced by curvature effects. Although the leading-edge flow separation, identified by instantaneous visualizations, seems to be a two-dimensional mechanism, the spanwise Reynolds stress dominates the other components in the upstream region of the bubble as the curvature increases. This striking feature is linked to the 3D nature of Kelvin-Helmholtz vortices. The maxima value of kinetic energy moves downstream toward the reattachment point as the curvature level decreases while high curvature cases produce higher levels of velocity fluctuations. This is also observed in the power spectra of streamwise velocity fluctuations from time series recorded further downstream the reattachment zone.

5. ACKNOWLEDGEMENTS

Present simulations have been performed using the supercomputers of GENCI at the IDRIS/CNRS and the CCRT. The authors are grateful to A. Spohn for his precious advices on this work.

6. REFERENCES

I. E. Abdalla and Z. Yang., 2004, "Numerical study of the instability mechanism in transitional separating-reattaching flow", *Int. J. Heat and Fluid Flow*, Vol.25, pp. 593–605.

S. Courtine, A. Spohn, and J.-P. Bonnet, 2007, "Vortex dynamics in the reattaching flow of separation bubbles with variable aspect ratio", In *Proc. of the 11th European Turbulence Conference, EUROMECH*, Porto, Portugal.

M. Kiya and K. Sasaki, 1985, "Structure of large-scale vortices and unsteady reverse flow in the reattaching zone of a turbulent separation bubble", *J. Fluid Mech.*, Vol. 154, pp. 463–491.

S. Laizet and E. Lamballais, 2009, "High-order compact schemes for incompressible flows: a simple and efficient method with the quasi-spectral accuracy", accepted for publication in *J. Comp. Phys.*.

S. Laizet, E. Lamballais, and J. C. Vassilicos, 2008, "A numerical strategy to combine high-order schemes, complex geometry and massively parallel computing for the dns of fractal generated turbulence", submitted to *Computers and Fluids*.

E. Lamballais, J. Silvestrini, and S. Laizet, 2008, "Direct numerical simulation of a separation bubble on a rounded finite-width leading edge", *Int. J. Heat and Fluid Flow*, Vol. 29, No. 3, pp. 612–625.

E. Lamballais, J. Silvestrini, and S. Laizet, 2009, "Direct numerical simulation of flow separation behind a rounded leading edge: stude of curvature effects", In *Proc. of the 6th International Symposium on Turbulence and Shear Flow Phenomena, TSFP-6*, Seoul, Korea.

P. Parnaudeau, J. Carlier, D. Heitz, and E. Lamballais, 2008, "Experimental and numerical studies of the flow over a circular cylinder at Reynolds number 3 900", *Phys. Fluids*, Vol 20(085101).

A. Suksangpanomrung, N. Djilali, and P. Moinat, 2000, "Large-eddy simulation of separated flow over a bluff rectangular plate", *Int. J. Heat and Fluid Flow*, Vol. 21, pp. 655–663.

Z. Yang and P. Voke, 2001, "Large-eddy simulation of boundary-layer separation and transition at a change of surface curvature", *J. Fluid Mech.*, Vol 439, pp. 305–333.

7. Responsibility notice

The author(s) is (are) the only responsible for the printed material included in this paper